

2-2011

# A batch-fabricated laser-micromachined PDMS actuator with stamped carbon grease electrodes

Teimour Maleki

*Birck Nanotechnology Center, Purdue University, tmalekij@purdue.edu*

Girish Chitnis

*Birck Nanotechnology Center, Purdue University, gchitnis@purdue.edu*

Babak Ziaie

*Birck Nanotechnology Center, Purdue University, bziaie@purdue.edu*

Follow this and additional works at: <http://docs.lib.purdue.edu/nanopub>



Part of the [Nanoscience and Nanotechnology Commons](#)

Maleki, Teimour; Chitnis, Girish; and Ziaie, Babak, "A batch-fabricated laser-micromachined PDMS actuator with stamped carbon grease electrodes" (2011). *Birck and NCN Publications*. Paper 1049.

<http://dx.doi.org/10.1088/0960-1317/21/2/027002>

This document has been made available through Purdue e-Pubs, a service of the Purdue University Libraries. Please contact [epubs@purdue.edu](mailto:epubs@purdue.edu) for additional information.

## A batch-fabricated laser-micromachined PDMS actuator with stamped carbon grease electrodes

This article has been downloaded from IOPscience. Please scroll down to see the full text article.

2011 J. Micromech. Microeng. 21 027002

(<http://iopscience.iop.org/0960-1317/21/2/027002>)

View [the table of contents for this issue](#), or go to the [journal homepage](#) for more

Download details:

IP Address: 128.46.221.64

The article was downloaded on 20/08/2013 at 18:49

Please note that [terms and conditions apply](#).

## TECHNICAL NOTE

# A batch-fabricated laser-micromachined PDMS actuator with stamped carbon grease electrodes

T Maleki<sup>1,2</sup>, G Chitnis<sup>2,3</sup> and B Ziaie<sup>1,2,4</sup><sup>1</sup> School of Electrical and Computer Engineering, Purdue University, West Lafayette, IN, USA<sup>2</sup> Birck Nanotechnology Center, Purdue University, West Lafayette, IN, USA<sup>3</sup> School of Mechanical Engineering, Purdue University, West Lafayette, IN, USAE-mail: [bziaie@purdue.edu](mailto:bziaie@purdue.edu)

Received 3 October 2010, in final form 16 December 2010

Published 18 January 2011

Online at [stacks.iop.org/JMM/21/027002](http://stacks.iop.org/JMM/21/027002)

## Abstract

In this note, we report on the development of a batch-fabricated laser-micromachined elastomeric cantilever actuator composed of a polydimethylsiloxane (PDMS) bilayer (active/inactive) and soft-lithographically patterned conductive carbon grease electrodes. The described unimorph structure has a low actuation voltage and large out-of-plane displacement. For a 4 mm long, 1 mm wide, and 80  $\mu\text{m}$  thick actuator, an out-of-plane displacement of 1.2 mm and a maximum force of 25  $\mu\text{N}$  were measured using 450 V actuation voltage.

(Some figures in this article are in colour only in the electronic version)

## 1. Introduction

Out-of-plane actuators are essential elements in many MEMS and microrobotic platforms [1–3]. Elastomeric actuators are an emerging class of electromechanical transducers that are not only inexpensive and lightweight but also have the ability to emulate the biological muscle in achieving high fracture toughness, large actuation strain, and inherent vibration damping [4–6]. Efforts in this area have been devoted toward reducing the actuating voltage and increasing the strain through various mechanical modifications (e.g., pre-stretching). Although some out-of-plane elastomeric actuators have been reported, they are mostly handmade and require a complicated fabrication process involving stretch frames and pre-patterned dome-shape elastomers [7, 8]. In this note, we report on the development of a batch-fabricated laser-micromachined unimorph elastomeric actuator with large out-of-plane displacement.

The operational principle of the elastomeric unimorph actuator is illustrated in figure 1(a). The actuator consists of a top active and a bottom inactive layer. The active layer is a dielectric elastomer film sandwiched between

two compliant electrodes. Applying a voltage between the compliant electrodes, which are in intimate contact with the active polymer film, induces a thickness compression and a lateral/transverse stretch. The bending moment generated henceforth in the bilayer combination bends the cantilever in the direction demonstrated by the green arrow shown in figure 1(a). A more detailed schematic of the actuator is depicted in figure 1(b). The active and inactive layers are made of PDMS with conductive grease serving as electrodes. An advantage of using PDMS as the actuator material is the ability to change its Young's modulus through simple chemical modifications (more crosslinker results in stiffer PDMS) [9]. Conductive carbon grease (CW7200BLK, Chemtronics Circuitworks, GA, USA) is chosen as the electrode due to its good adhesion to PDMS and low deformation resistance.

## 2. Design and simulation

Maxwell strain generated in the active layer upon the application of a voltage across the electrodes is given by [6]

$$e_h = \frac{\Delta h_1}{h_1} = -\frac{1}{Y_1} \varepsilon \varepsilon_0 E^2 = -\frac{1}{Y_1} \varepsilon \varepsilon_0 \left( \frac{V}{h_1} \right)^2, \quad (1)$$

<sup>4</sup> Author to whom any correspondence should be addressed.

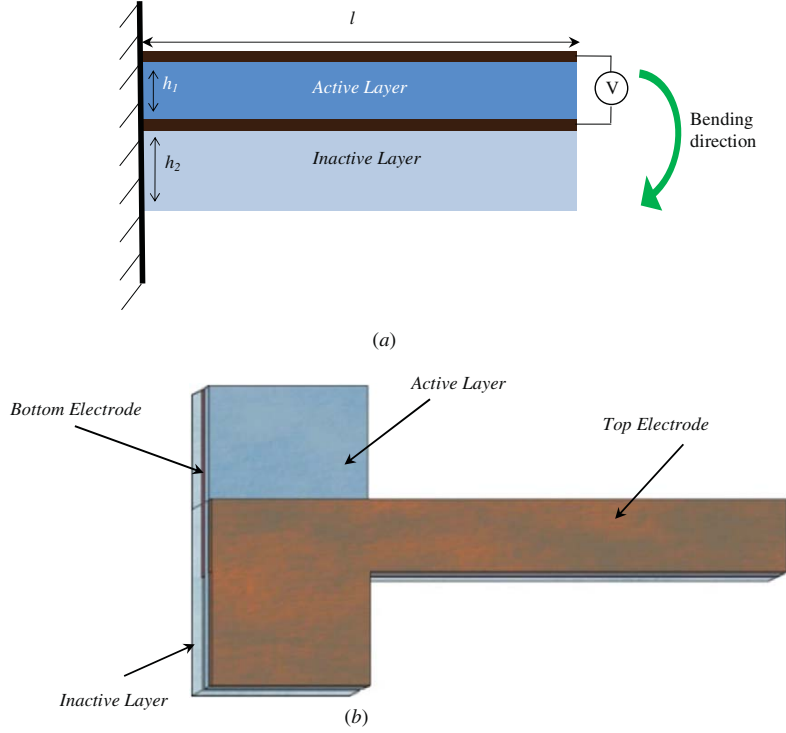


**Figure 1.** (a) Cross section schematic of the elastomeric unimorph actuator, (b) a more detailed view showing different layers.

where  $h_1$  and  $Y_1$  are the thickness and Young's modulus of the active layer, respectively,  $\varepsilon$  is the active layer dielectric constant,  $\varepsilon_0$  is air electric permeability,  $E$  is the applied electric field, and  $V$  is the applied voltage. Unlike conventional electrostatic air gap actuators, in elastomeric ones, the expanding area of electrodes in the lateral direction also contributes to the generated force [10].

The induced longitudinal strain of the active layer  $e_l$  can be written as [11]

$$e_l = \frac{\Delta l}{l} = -\frac{e_h}{\left(\frac{Y_2 w_2 h_2}{Y_1 w_1 h_1} + 1\right)}, \quad (2)$$

in which  $l$  is the length of the beam, and  $h_2$ ,  $Y_2$ , and  $w_2$  are the thickness, Young's modulus, and the width of the inactive layer, respectively. Due to the presence of the inactive layer, the transverse contraction and its associated longitudinal expansion induce a bending moment in the cantilever resulting in an out-of-plane deflection for which the curvature of the beam,  $K$ , is given by [11]

$$K = \frac{6h_2(h_1 + h_2)\varepsilon\varepsilon_0 V^2}{Y_1 h_1 \left[ \alpha h_1^4 + 2h_1 h_2 (2h_1^2 + 3h_1 h_2 + 2h_2^2) + \frac{h_2^4}{\alpha} \right]}, \quad (3)$$

where

$$\alpha = \frac{Y_1 w_1}{Y_2 w_2}. \quad (4)$$

As can be seen from equation (3), the curvature and hence the deflection ( $K$  is proportional to the deflection) depends not only on the applied voltage ( $V^2$ ) but also on the active and inactive layers' thicknesses ( $h_1$  and  $h_2$ ) and their Young's

moduli ( $Y_1$  and  $Y_2$ ). However, due to the higher power terms in the denominator of equation (3), the dependence on the layer thicknesses is stronger than that of Young's moduli.

Comsol Multiphysics<sup>TM</sup> finite element simulation was used to estimate the displacement versus applied voltage and other structural parameters. Figure 2(a) shows the simulation results for a 1 mm wide cantilever with three different lengths (3, 4, and 5 mm) assuming 20 and 50  $\mu\text{m}$  thick active and inactive layer thicknesses (for PDMS,  $Y = 750$  kPa and  $\varepsilon = 2.7$ ). As expected, the displacement versus voltage is nonlinear and one can easily achieve mm-scale deflections with a modest actuation voltage, equation (3). Figure 2(b) shows the displacement versus normalized layer thicknesses (i.e.  $h_2/h_1$  assuming 20  $\mu\text{m}$  active layer thickness) when the active layer is actuated with 450 V. For  $h_2/h_1 > 15$ , all three curves merge and result in a negligible deflection. This is expected since by ignoring smaller terms (i.e. ignoring  $h_1$  with respect to  $h_2$  when  $h_2/h_1 > 15$ ) in the denominator of equation (3), the beam curvature can be approximated by (assuming  $\alpha = 1$ )

$$K \cong \frac{6\varepsilon\varepsilon_0 V^2}{Y_1 h_1 h_2^2}, \quad (5)$$

indicating a small curvature and hence a small tip deflection. For the smaller  $h_2/h_1$  ratio (i.e.  $h_2/h_1 < 5$ ), several terms in the denominator have the same orders of magnitude (the last three terms) resulting in a larger curvature and tip deflection.

To estimate the effect of stiffness variations on the actuator performance, we simulated several structures (3, 4, and 5 mm long beams with 20 and 50  $\mu\text{m}$  thick active and inactive layer

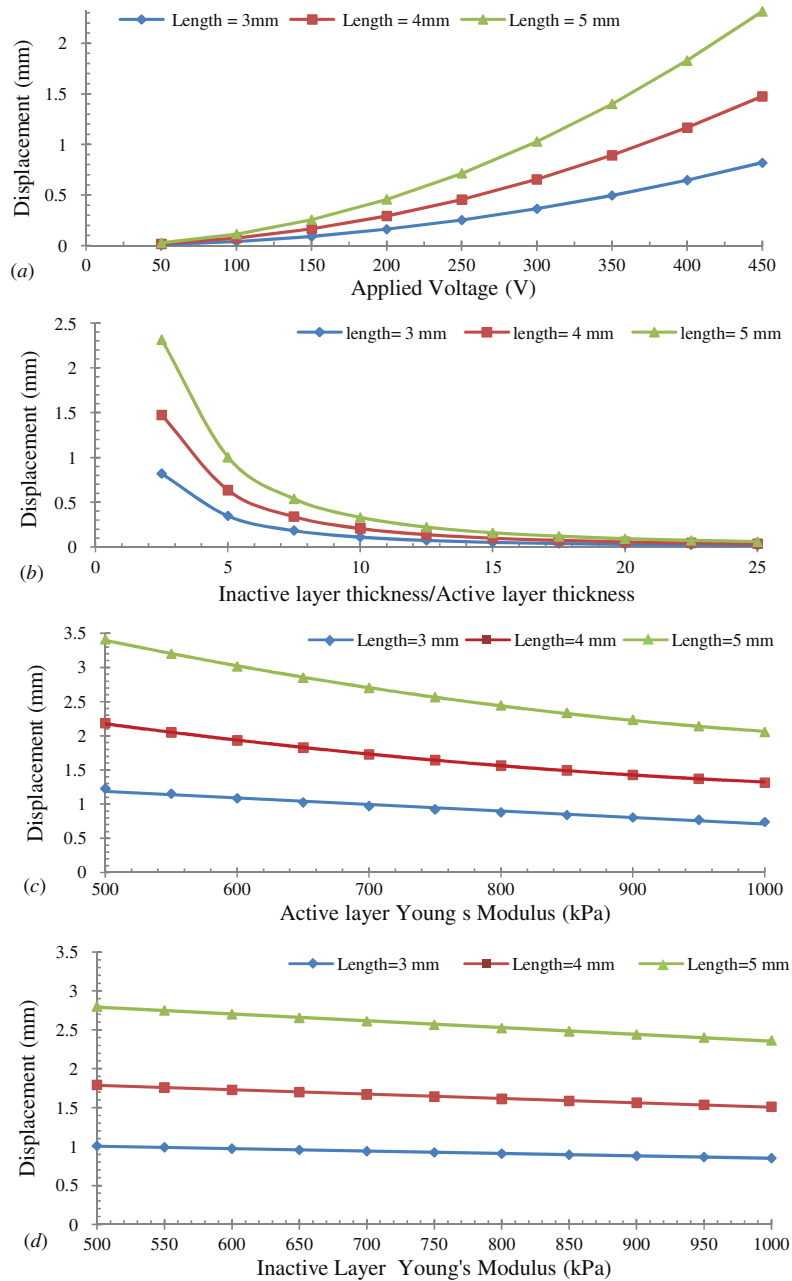


**Figure 2.** Comsol™ simulation results for an elastomeric unimorph actuator made of PDMS, (a) displacement versus voltage for a PDMS actuator with a 50  $\mu\text{m}$  thick inactive and a 20  $\mu\text{m}$  thick active layer, (b) deflection versus inactive/active layer thickness ratio, (c) displacement versus active layer's Young's modulus, and (d) displacement versus inactive layer's Young's modulus.

thicknesses when actuated by 500 V) with Young's modulus variations of 100%. As shown in figure 2(c), a 100% change in the active layer's Young's modulus (inactive layer's Young's modulus = 750 kPa) can change the output displacement by more than 50%, while the effect of the inactive layer's Young's modulus (active layer's Young's modulus = 750 kPa) on deflection is much less, figure 2(d). These simulations suggest that for a given voltage, it is advantageous to decrease the active layer's Young's modulus while simultaneously increase

that of the inactive layer. This ensures a maximum output displacement for an increased actuator rigidity and output force.

### 3. Fabrication process

Figure 3 illustrates the fabrication process incorporating several important steps to ensure batch processability. These include soft lithography for printing the electrodes and

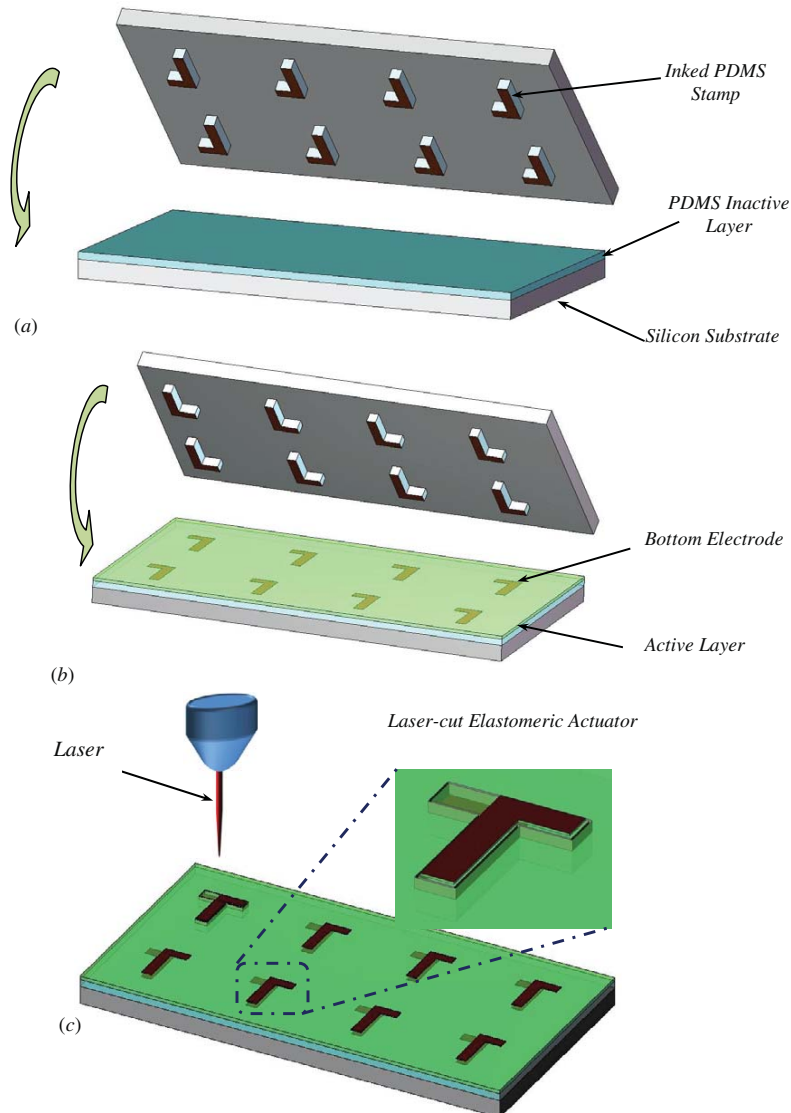


**Figure 3.** Fabrication process for the elastomeric actuator, (a) stamping the bottom electrode on top of the spun-coated inactive PDMS layer, (b) stamping the top electrode on top of the spun-coated active PDMS layer, and (c) final separation of individual actuators by laser micromachining.

batch separation using laser micromachining. The process starts with a  $300\ \mu\text{m}$  thick SU-8 (SU-8 2100, MicroChem) on a silicon wafer mold onto which the electrode PDMS stamp (Sylgard 184, Dow Corning, mixing ratio = 10:1) is cast and subsequently separated. Then, a thin layer of conductive carbon grease is prepared on a flat PDMS layer and electrode stamp is inked against it. The  $50\ \mu\text{m}$  thick inactive PDMS layer is then spun coated on a pretreated silicon wafer (tridecafluoro-(1,1,2,2-tetrahydrooctyl)-1-trichlorosilane, United Chemical Technologies, Inc.) and cured at  $100\ ^\circ\text{C}$  for 15 min. Subsequently, the first L-shaped electrode layer (described above) is stamped onto the inactive PDMS layer, figure 3(a). Afterward, a  $25\ \mu\text{m}$  thick PDMS (15:1 ratio to decrease Young's modulus and hence increase

the deflection) layer is spun on top to act as the active layer. This is followed by alignment and stamping of the top L-shaped electrode, figure 3(b). Finally, individual actuators are separated at the wafer level by using laser micromachining, ( $\text{CO}_2$  laser generated by 2007 Professional Systems from Universal Laser Systems Inc., AZ, USA), figure 3(c). Each cantilever could be separated from the silicon substrate using a tweezer since the PDMS has minimal adhesion to the pretreated substrate. Figure 4(a) shows a wafer with an array of actuators that has been separated using laser micromachining. The magnified image in figure 4(a) represents a single actuator achieved by PDMS laser micromachining. Figure 4(b) shows a single actuator mounted on a block of PDMS for test and characterization. The fabricated actuators can be

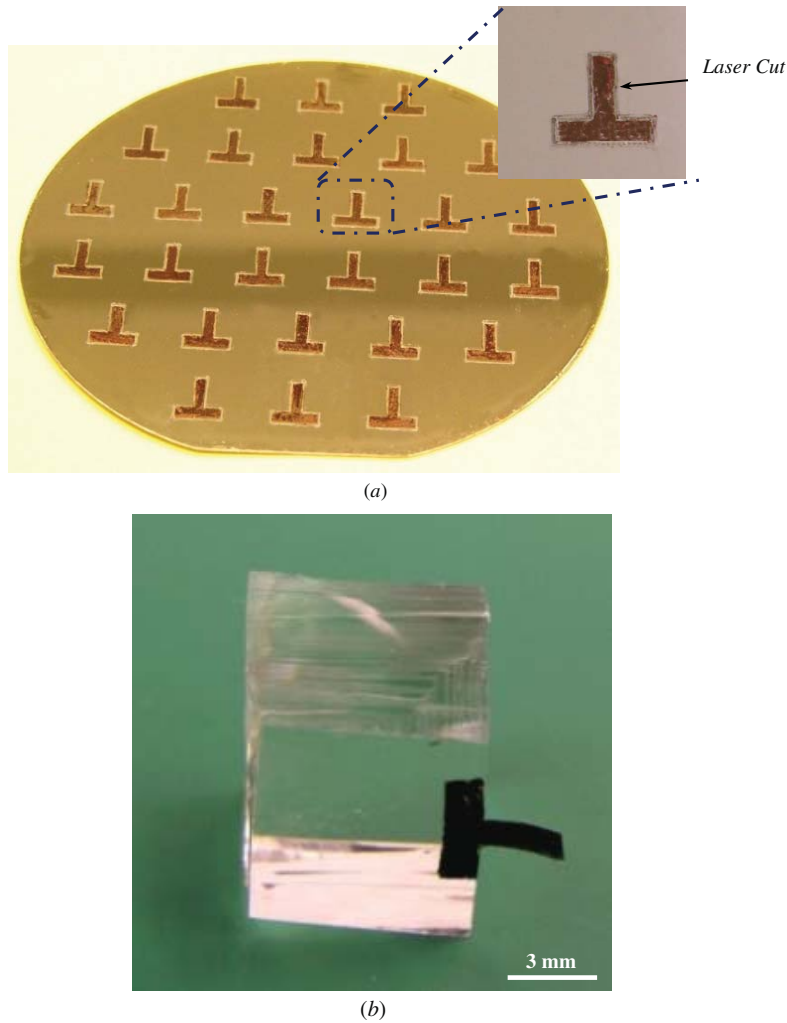


**Figure 4.** (a) Batch fabricated elastomeric actuators on a silicon wafer after separation by laser micromachining; magnified image shows the laser cutting orientation; (b) measurement setup, a single actuator was mounted on a PDMS block.

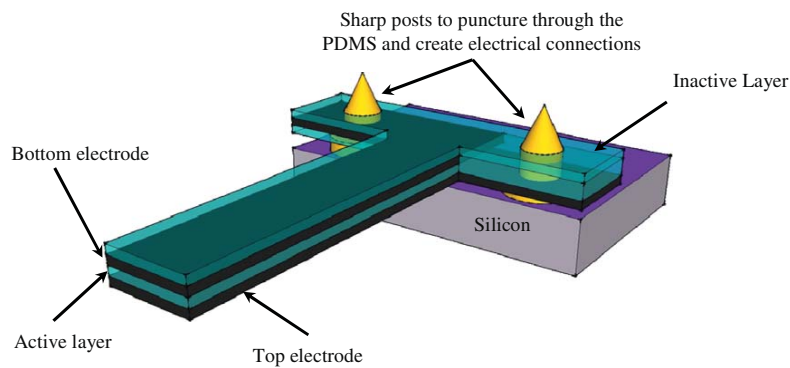


**Figure 5.** Cross-sectional schematic of a possible scheme for incorporation of elastomeric actuators with MEMS technology using sharp posts (e.g., gold stud bumps) to establish electrical contacts.

incorporated into MEMS systems through the pick-and-place method. Figure 5 shows a possible design in which the contact electrodes are sharp enough to penetrate through the

PDMS layer (e.g., a gold stud bump). These contacts could also be used to act as an anchor, holding the actuator in its position.

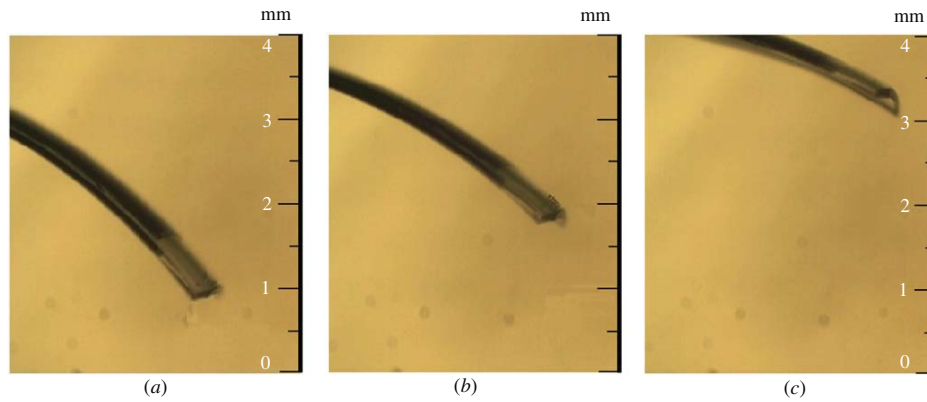


Figure 6. Optical images of an 80  $\mu\text{m}$  thick, 1 mm wide, and 5 mm long actuator with: (a) 0 V, (b) 250 V, and (c) 500 V applied voltage.

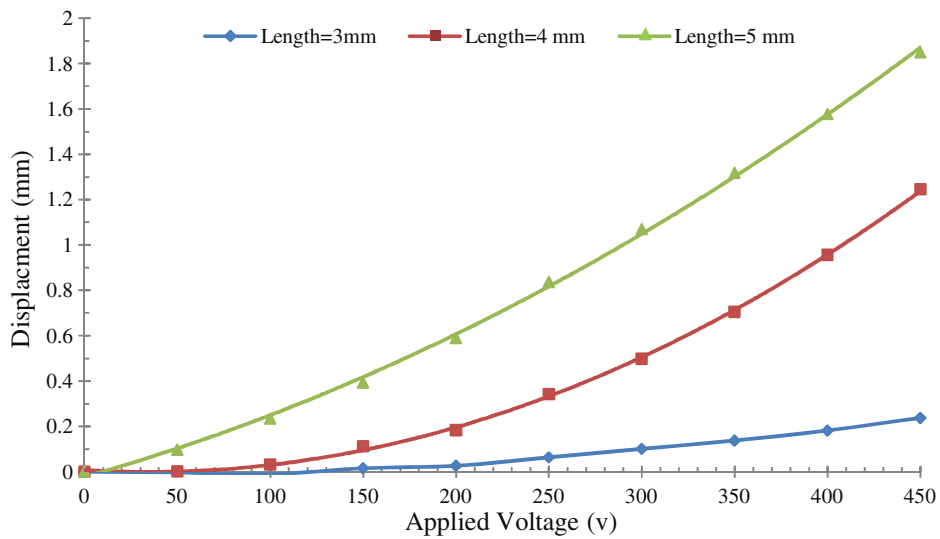


Figure 7. Measurement results showing out-of-plane displacement versus actuation voltage for a 1 mm wide, 80  $\mu\text{m}$  thick elastomeric actuator with three different lengths.

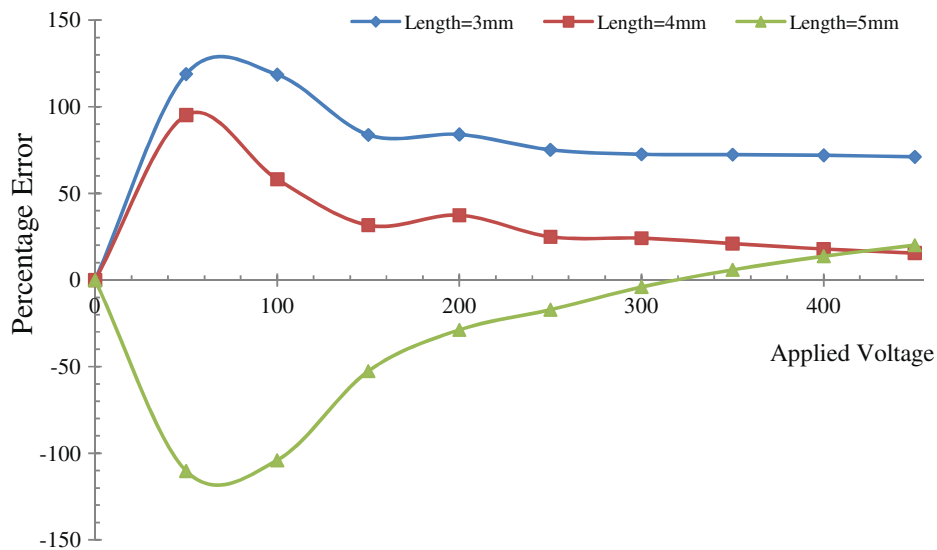
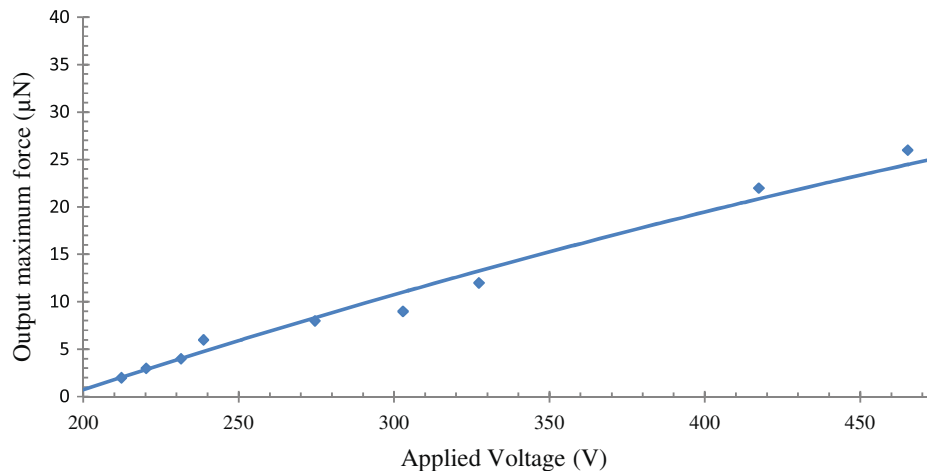


Figure 8. Percentage error between simulated and experimental values of the actuator deflection versus applied voltage.



**Figure 9.** Actuation voltage versus maximum force for a 4 mm long, 1 mm wide, and 80  $\mu\text{m}$  thick elastomeric actuator.

#### 4. Experimental results

After fabrication, the actuators were mounted on a PDMS block and electrical connections were established by punching needle probes through the PDMS layers. Actuators were tested using a high voltage power supply and their displacement was measured through a video frame-grabber. Optical pictures of a 5 mm long actuator at different actuation voltages are depicted in figure 6. Figure 7 shows tip-displacement versus applied voltage for a 1 mm wide elastomeric actuator with three different lengths (3, 4, and 5 mm). As can be seen, mm-scale actuation was achieved for voltages less than 500 V. To evaluate the experimental results against the simulation, the percentage error in the deflection, defined as  $100 \times (D_{\text{Simulated}} - D_{\text{Experimental}}) / D_{\text{Simulated}}$ , is plotted in figure 8. As can be seen, when the deflection is large, the experimental results closely follow the simulations for the 4 and 5 mm cantilevers while for the 3 mm actuator the deflection is less than the simulated results. This can be attributed to the experimental setup, specifically the effect of punching needles for electrode contacts (needle penetration on the backend shortens the cantilever to some extent; this is more noticeable at smaller deflections as well as the shorter cantilevers (3 mm cantilever) at larger deflections). In another set of experiments, the maximum output force (clamped condition) versus applied voltage was measured for a 4 mm long actuator, and the result is plotted in figure 9. A maximum force of 25  $\mu\text{N}$  was achieved using a 450 V actuation voltage.

#### 5. Conclusions

In conclusion, we designed, simulated, and characterized a batch-fabricated laser-micromachined elastomeric actuator with low actuation voltage and large out-of-plane deflection. Simulation results indicated that one can achieve large deflections by using a soft active layer, while having a reasonable stiffness by using a stiffer inactive layer. Furthermore, to achieve higher deflection, it is important to

keep the ratio of the inactive to active layer thickness to be less than 5. Three different size actuators were successfully fabricated using this method and their performances were characterized. Millimeter-scale out-of-plane displacement was achieved using a fairly low voltage (less than 500 V). A 4 mm long actuator was capable of applying 25  $\mu\text{N}$  force using 450 V actuation voltage.

#### Acknowledgments

The authors would like to thank the staff at the Birck Nanotechnology Center, Purdue University for their assistance in fabrication. They would also like to thank Professor Cagri Cavran and Dr Chun-Li Chang for their help with laser micromachining.

#### References

- [1] Michael A, Kwok C Y, Yu K and Mackenzie M R 2008 A novel bistable two-way actuated out-of-plane electrothermal microbridge *J. Microelectromech. Syst.* **17** 58–68
- [2] He S and Mrad R B 2008 Design, modeling, and demonstration of a MEMS repulsive-force out-of-plane electrostatic micro actuator *J. Microelectromech. Syst.* **17** 532–47
- [3] Ren K, Liu S, Lin M, Wang Y and Zhang Q M 2008 A compact electroactive polymer actuator suitable for refreshable Braille display *Sensors Actuators A* **143** 335–42
- [4] Plante J-S and Dubowsky S 2007 On the properties of dielectric elastomer actuators and their design implications *Smart Mater. Struct.* **16** S227–36
- [5] Löwe C, Zhang X and Kovacs G 2005 Dielectric elastomers in actuator technology *Adv. Eng. Mater.* **7** 361–7
- [6] O'Halloran A, O'Malley F and McHugh P 2008 A review on dielectric elastomer actuators, technology, applications, and challenges *J. Appl. Phys.* **104** 071101
- [7] Kornbluh R, Pelrine R, Pei Q, Heydt R, Stanford S, Oh S and Eckerle J 2002 Electroelastomers: applications of dielectric elastomer transducers for actuation, generation and smart structures *Proc. SPIE* **4698** 254–70

- [8] Carpi F, Frediani G, Mannini A and De Rossi D 2008 Contractile and buckling actuators based on dielectric elastomers: devices and applications *Adv. Sci. Technol.* **61** 186–91
- [9] Brown X Q, Ookawa K and Wong J Y 2005 Evaluation of polydimethylsiloxane scaffolds with physiologically-relevant elastic moduli: interplay of substrate mechanics and surface chemistry effects on vascular smooth muscle cell response *Biomaterials* **26** 3123–9
- [10] Krakovsky I, Romijn T and Posthuma de Boer A 1999 A few remarks on the electrostriction of elastomers *J. Appl. Phys.* **85** 628–9
- [11] Costen R C, Su J and Harrison J S 2001 Model for bending actuators that use electrostrictive graft elastomers *Proc. SPIE* **4329** 437–44